




Article

Implementation of Antibacterial Nanoparticles in Additive Manufacturing to Increase Part Strength and Stiffness

Christopher Billings¹, Peter Kim², Tyler Shadid³, Jimmy D. Ballard^{3,*}, Changjie Cai^{2,*} and Yingtao Liu^{1,*} 

¹ School of Aerospace and Mechanical Engineering, University of Oklahoma, Norman, OK 73019, USA

² Department of Occupational and Environmental Health, The University of Oklahoma Health Sciences Center, The University of Oklahoma, Oklahoma City, OK 73104, USA

³ Department of Microbiology, The University of Oklahoma Health Sciences Center, The University of Oklahoma, Oklahoma City, OK 73104, USA

* Correspondence: jimmy-ballard@ouhsc.edu (J.D.B.); changjie-cai@ouhsc.edu (C.C.); yingtao@ou.edu (Y.L.)

Abstract: The introduction of novel composites suited for additive manufacturing machines offers a solution for the current slow adoption of the technology. Many composites offer secondary functions and mechanical improvements to suit unique applications better. This article presents the creation of a set of novel nanocomposites consisting of zinc oxide (ZnO) and a photocurable resin using a masked stereolithography additive machine. These nanocomposites are produced in 1%, 2.5%, 5%, and 7.5% concentrations and are characterized based on their mechanical and surface properties. Using ZnO allows for the creation of mechanically stronger parts with reduced wettability while offering antibacterial properties throughout the entire part. Best results were observed at a 5% concentration of ZnO with a nearly 25% strength increase and 45% decrease in wettability. Additionally, SEM analysis demonstrated proper dispersion with minimal agglomerations present. In the sporicidal effect analysis, the ZnO (with 7.5% concentration) reduced 31.5% of *Clostridioides difficile* spores. These results demonstrate the capability of producing antibacterial nanocomposites using low-cost additive manufacturing to enhance public health options.

Keywords: additive manufacturing; masked stereolithography; zinc oxide; photocurable nanocomposite; *Clostridioides difficile*; sporicidal effects



Citation: Billings, C.; Kim, P.; Shadid, T.; Ballard, J.D.; Cai, C.; Liu, Y. Implementation of Antibacterial Nanoparticles in Additive Manufacturing to Increase Part Strength and Stiffness. *J. Compos. Sci.* **2022**, *6*, 248. <https://doi.org/10.3390/jcs6090248>

Academic Editor: Francesco Tornabene

Received: 19 July 2022

Accepted: 23 August 2022

Published: 25 August 2022

Publisher's Note: MDPI stays neutral with regard to jurisdictional claims in published maps and institutional affiliations.



Copyright: © 2022 by the authors. Licensee MDPI, Basel, Switzerland. This article is an open access article distributed under the terms and conditions of the Creative Commons Attribution (CC BY) license (<https://creativecommons.org/licenses/by/4.0/>).

1. Introduction

The production of composites in additive manufacturing is limited to very few specialty machines. It is accepted that one of the best ways to incorporate composites into additive manufacturing is by introducing composite resins [1]. The primary benefit to this type of composite is that it often requires little to no modification of the printing system. Additionally, the use of resins allows for printing at high resolutions to rival the quality of traditional manufacturing. The disadvantage is that many resins suffer from limited mechanical performance and are produced at high viscosity, making it challenging to introduce a fiber composite into the matrix [2]. Currently, researchers are working to help develop smart materials and characterize novel resins to solve this gap [3].

Composites have been successfully produced utilizing additive manufacturing techniques, including fused deposition modeling, direct ink writing, selective laser sintering, and stereolithography (SLA) [4–7]. SLA-based manufacturing produces high-resolution parts capable of withstanding various environmental factors due to its photopolymerization process, where the chemicals crosslink to produce the final part [8]. These benefits create a strong case for experimenting with high-resolution nanocomposites that offer beneficial functionality. The nature of photopolymerization does not require high temperatures compared to other additive manufacturing processes, and therefore, allows for a wider variety of reinforcements. Additionally, the resolution of this manufacturing process is often under 25 microns [8]. This high resolution paired with a wide range of compatible fillers creates

an ideal environment for producing medical prototypes, geometry-restricted parts, and parts with opacity requirements that cannot be traditionally manufactured.

To maximize the applications of this high-resolution additive manufacturing technology, it is critical to add a reinforcement that offers beneficial functions. Zinc oxide (ZnO) nanoparticles have been widely applied due to their controllable nanostructures, morphology, synthesis methods, and even antibacterial properties [9–14]. Extensive research has been performed on the antibacterial effects of ZnO as nanoparticle sizing changes [15]. These studies have focused on the effect of nanoparticle size on antibacterial effectiveness, demonstrating that a decrease in particle size leads to an increase in antibacterial activity [16–19]. These studies help guide future use of the material and highlight the importance of proper dispersion of ZnO when being implemented for its antibacterial properties.

The antibacterial properties have been well documented, and research has shown that it is effective against many items such as the SARS-CoV-2 virus [20]. The ZnO used in many of these studies also demonstrated a positive correlation between UV light exposure and antibacterial performance [21]. These results provide a foundation for utilizing the ZnO as a filler in a UV-activated photopolymer, as the ZnO should not be harmed in the manufacturing process. However, to our knowledge, no studies focused on the sporicidal effects of ZnO nanocomposites on *C. difficile* spores, which is the leading cause of nosocomial diarrhea worldwide with substantial morbidity, mortality and healthcare cost [22].

A concern when utilizing ZnO in a photocurable resin is the UV absorbance characteristics of the material. Research has shown that ZnO is naturally UV absorbent and increasingly absorbent at a range of 15–40 nm [23,24]. This creates a problem when compounded with the antibacterial effectiveness also increasing as particle size decreases. When ZnO was introduced into other thermosets, such as epoxy nanocomposites, studies found that it had an adverse effect on cure time and overall cure strength [25]. Properly adjusting post-curing time and in-process cure time will be required to overcome the UV absorption caused by the ZnO. Studies done on control resins have demonstrated that the post-curing of the material has a significant effect on the strength but does not affect the middle layers, and therefore attention to the in-process curing will be critical [26].

With the production of antibacterial parts, it will be important to characterize the wettability properly. Parts that harbor moisture will lead to more significant issues relating to bacterial growth, so a low wettability would be desired. As the novel nanocomposite will functionally always have a ZnO coating, the surface energy of the ZnO will play a prominent role in the final part's wettability. Studies performed on ZnO's wettability have shown that it can be highly hydrophobic under the correct conditions [27,28]. The integration of the ZnO and activation of it through UV exposure will again be essential to achieve the desired characteristics.

Increasing the strength of a composite will often increase the wear resistance of a material. A study on the wear resistance of resin printing found that it was similar to the bulk materials obtained during traditional manufacturing, so any improvements would be advantageous [29]. Previous work on this topic with several different matrix materials demonstrated an increase in wear resistance when zinc oxide nanoparticles were introduced at concentrations of 1% [30]. These results rely heavily on reducing voids in the final printed part.

Previous research has defined the need for composites in additive manufacturing. Zinc oxide was selected to form a nanocomposite due to its various chemical and mechanical functions. The extensive documentation on these characteristics allows for focusing on developing the nanocomposite and testing the printed parts. A masked SLA printing system was selected due to its high resolution, low entry cost, and liquid material.

2. Materials and Methods

The additive manufacturing system utilized to produce the samples was an Elegoo Mars 2 Pro masked stereolithography (MSLA) printer. MSLA and direct light processing (DLP) curing systems often suffer from light leaks around the LCD. A monochrome LCD

is implemented in the Mars 2 Pro to increase light transmission and help with the above issues. The base matrix material was a standard photopolymer from Elegoo in grey coloring. The resin is composed of epoxy resins, hexamethylene diacrylate, N-glycine, and hydroxy cyclohexyl phenyl ketone. This was chosen due to the low viscosity of the material relative to other low-cost options and the quick cure times when paired with their respective machine.

The nanoparticle of choice was zinc oxide sized between 10–30 nanometers from US Research Nanomaterials Inc., Houston, TX, USA. Zinc oxide was chosen due to its antibacterial properties, use in human-safe products, and low cost. In addition, the part will require complete dispersion of the nanoparticle throughout to exhibit antibacterial properties; therefore, several different concentrations were tested to analyze the particle’s effect on the part’s physical properties.

To fabricate the novel nanocomposite slurry, the nanoparticle was added to the matrix resin in the following weight concentrations: 1%, 2.5%, 5%, and 7.5%. The nanoparticle was dispersed throughout the matrix material through a high-speed centrifugal mixer to reduce agglomeration, as demonstrated through SEM later in the manuscript. An AR-100 Thinky mixer was used at a setting of 5 min of mixing and 2 min of degassing for all mixtures utilizing a centrifugal process for air removal. This process also heated the material due to the process’s friction and decreased the viscosity of the final mixture. This aided in the reduction in trapped air molecules when transferring the mixture to the printing vat. Once loaded into the printer, the custom print settings were uploaded, and the print was started. After 10 min of printing, the print was paused to ensure the part had adequately adhered to the build plate. If so, the print was left to resume to completion and removed for post cleaning and curing. The entire process is depicted in Figure 1 below of the fabrication and manufacturing of the novel resin material.

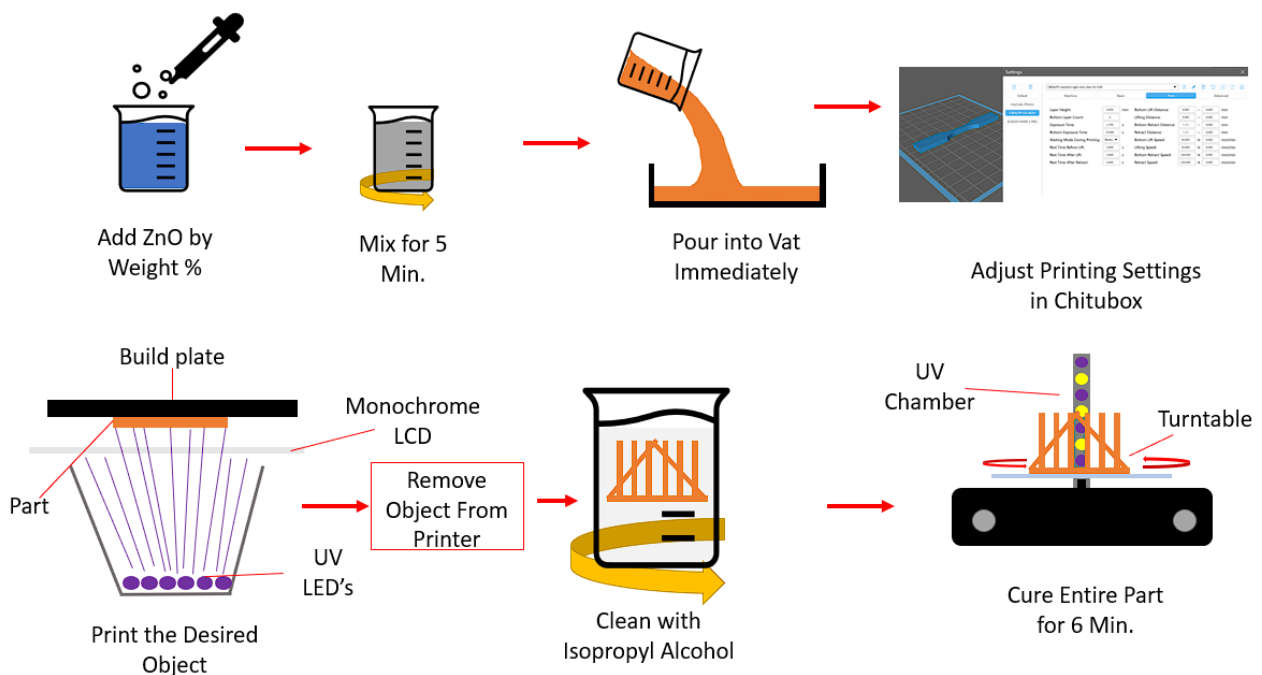


Figure 1. The manufacturing process for ZnO nanocomposite resin.

Proper particle dispersion is a substantial problem when working with nanoparticles of this size. Utilizing a low viscosity resin is ideal for helping aid the overall particle dispersion, but heating the material also proved advantageous to the mixing process. The resin was heated on a hot plate at 60 °C and then left to cool to room temperature. This resin was then utilized in the printer with no adverse effects on the printing process. This data was then used to help set mixing times based on the change in viscosity due to the

thermal change of the material. Mixing times of 2 min led to insignificant changes in matrix temperature, and large agglomerations were still visible. Increasing this mixing time to the 5 min mark while adding a degassing phase solved these problems. This procedure reduced the overall viscosity of the resin at all concentrations to a value lower than the control matrix at room temperature while completely dispersing the nanoparticle, as later demonstrated through SEM. When mixing for a longer duration, substantial air pockets were formed in the nanocomposite. A 2 min degassing phase on the Thinky mixer was incorporated to remove these air pockets.

The selected matrix utilizes isopropyl alcohol as a solvent, so all parts were rinsed thoroughly when removed from the printer. This ensured that inspected parts did not contain ZnO on the surface due to inadequate cleaning, but the nanoparticle was deposited within the part during the printing process. To obtain reliable antibacterial testing, it was critical to ensure that the ZnO reacting with the bacteria was adequately bonded to the part and not simply attached to the surface. Thorough cleaning with a solvent ensured that the only ZnO left exposed to the surface was adequately bonded and, therefore, would wear over time alongside the matrix.

Characterization of the mechanical properties of the nanocomposite was performed through testing of tensile specimens that would be printed for each variation of material. The printer was unmodified to produce the tensile specimens for testing, and all samples were printed at 22 °C. To achieve proper printing of the nanocomposite, cure times were adjusted based on the concentration of the nanoparticle, as shown in Table 1. To determine optimal cure times, the nanocomposite was printed using control settings, and cure times were gradually increased until print failures were no longer present. ZnO is often utilized for its UV absorption characteristics. Therefore, the cure time had to be increased accordingly to cure the photopolymer around the particles. To ensure that this change in cure time during the printing process did not affect the final strength, all samples were exposed to UV light in a chamber for a minimum of six minutes after removal from the printer. This should negate any difference in strength gained during the curing inside the printer. The prints were composed of two distinct layer settings. These layers refer to the first five layers produced by the printer and then any layer printed after that. There was no change in the dimension of these layers, but the cure times were changed to aid in creating a solid foundation for the part to print on. The bottom layers physically bond to a stainless-steel sheet and, therefore, must be more completely cured to support the rest of the print. The remaining layers are cured at much shorter times to allow the curing reaction to progress enough for the part to hold its geometry but still require post-UV treatment. This dramatically reduces print time and allows for easier post-processing, such as support removal. A total of five bottom layers were used on all parts, with a total layer count of 33.

Table 1. Cure Settings for All Different Novel Nanocomposites.

Weight %	Bottom Cure Time (S)	Normal Cure Time (S)
0%	30	2.5
1%	35	3
2.5%	40	3.5
5%	50	5
7.5%	60	8

To test the tensile strength of the specimens, an Instron 5969 was utilized with a constant strain rate of 1 mm/min. The tensile specimens were based on the ASTM D638 standard utilizing a barbell style with a gauge length of 40 mm, a gauge width of 10 mm, and a thickness of 1.75 mm. The testing machine utilized a 5 kn load cell, and all samples were tested with zero pretension and preload applied. A total of six specimens were tested for all concentrations to assess variability. These specimens were then analyzed under an optical microscope to determine the failure mode. An optical microscope image was

processed through ImageJ and tested across four samples to determine the water contact angle [31,32].

In order to test its sporicidal effects, we generated *C. difficile* spores using the VPI 10463 (a toxin A and toxin B positive strain) in the lab. *C. difficile* spores (12 uL) were resuspended in sterile water (4 mL), resulting the concentration of approximately 20,000 spores per mL. The solution was dispensed by 1 mL onto four discs, including (1) baseline, (2) control (with polymer only), and (3) ZnO nanocomposite. They were first sealed with parafilm and left for 24 h. Then, they were diluted in serial and were plated to input sample on Brain Heart Infusion Supplemented- Taurocholate Acid (BHIS-TCA). After another 24 h, spores and water were mixed on discs for 10 s. Serial dilution was repeated on BHIS-TCA. Finally, the colonies were counted. For spore cultivation, media was grown in an anaerobic environment chamber to prepare media for spore placing. Finally, we obtained three different colonies counting for each sample. ANOVA analysis with Tukey Multiple Comparison post hoc analysis were used to test the difference of *C. difficile* colony counts between each sample. The assumption of homogeneity of variance and normality was tested with Levene's test and Shapiro–Wilk test.

3. Results

To characterize each material in mechanical applications properly, tensile tests were performed with metrics on ultimate tensile strength, modulus, and strain. These samples were analyzed under a microscope to identify the failure mode and ensure it was not due to a defect in the printing process. Water contact angle measurements were performed and characterized across all samples to analyze changes in surface energy. This data was paired with SEM imagery to characterize the particle dispersion on the surface. SEM images were analyzed using particle analysis to provide insights into agglomeration size, with EDS being utilized to verify the ZnO concentration.

3.1. Tensile Testing

For the six control samples consisting of only the matrix material, an average stress of 31.6 MPa was demonstrated with Young's modulus of 118.8 MPa. These statistics reveal that the base matrix performs similarly to the commonly used ABS thermoset when under load with an increased strain [33]. An increase in the ultimate tensile stress and modulus would be expected to improve the practical use of the matrix.

Starting with the 1% ZnO nanocomposite, all mechanical parameters were reduced. Stress was reduced by ~15%, while strain increased by ~44%. These parameters reduce the practical applications of the material and eliminate the usefulness of a nanocomposite with a ZnO concentration of 1%

At 2.5% ZnO concentration, an increase in parameters was noted from the 1% specimens. These samples performed statistically similar to the control group, with an average ultimate tensile stress of 30.3 MPa and modulus of 848.2 MPa. More importantly, is a reduction in standard deviation for both parameters across all samples.

The maximum increase in ultimate tensile strength was observed at the 5% ZnO concentration with a value of 39.5 MPa. This is a ~25% increase compared to the control matrix. Additionally, a 36% increase was observed in the material modulus with a standard deviation over three times less than the control. These samples demonstrated the least amount of strain at only ~6% and had the least amount of strain deviation out of all samples tested.

The final 7.5% ZnO samples tested performed statistically similar to the 5% samples regarding tensile strength. However, degradation in modulus and the ultimate strain was observed with a modulus of 975.97 MPa. The average strain of these samples was statistically identical to the control and 2.5% samples at ~6%. The ultimate tensile strength and modulus of all samples was graphed in Figure 2. When visually compared, it is relevant to note the increase in standard deviation for ultimate tensile stress as ZnO concentration increases. However, this is the opposite for the modulus, as the lowest standard deviation

amounts were observed in the 5% and 7.5% samples. This trend allows for insights into the mechanical function of ZnO in terms of stiffness and strength addition and leads to better theories on the fracture mechanism of the material. All mechanical data along with standard deviation are presented in Table 2.

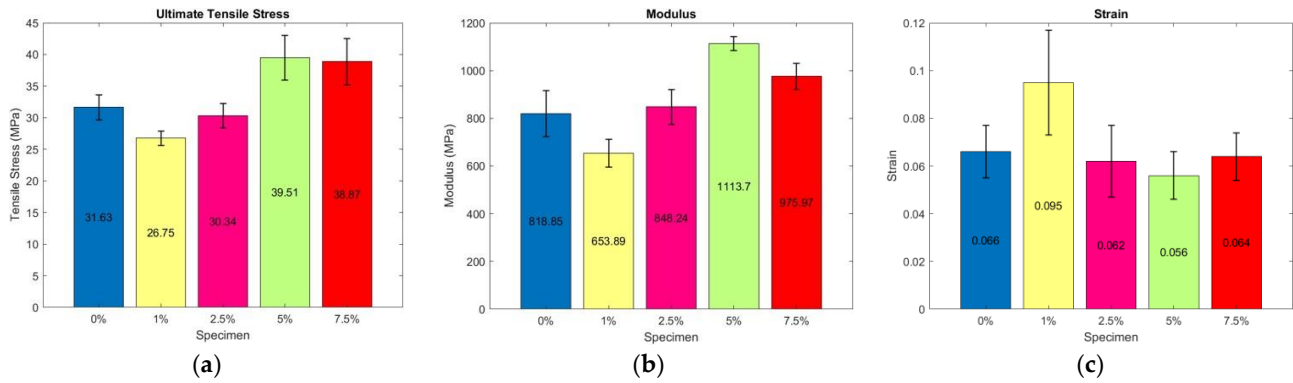


Figure 2. (a) Average ultimate tensile stress with error bars representing standard deviation. (b) Average modulus with error bars representing standard deviation. (c) Average strain with error bars representing standard deviation.

Table 2. Stress, strain and modulus data for all samples including standard deviation.

Weight %	Stress (MPa)	Strain	Modulus (MPa)
0%	31.6 ± 2	0.066 ± 0.01	818.85 ± 96.37
1%	26.8 ± 1.2	0.095 ± 0.022	653.89 ± 58.73
2.5%	30.3 ± 1.9	0.062 ± 0.015	848.24 ± 73.39
5%	39.5 ± 3.5	0.056 ± 0.01	1113.70 ± 30.18
7.5%	38.9 ± 3.7	0.064 ± 0.009	975.97 ± 55.44

3.2. Water Contact Angles

To characterize surface quality and functions the ZnO provides, water contact angles were measured for each sample. As a baseline, the control showed a water contact angle of 48°, demonstrating hydrophilic properties. Any increase in the contact angle would be beneficial as it would help reduce the amount of moisture that would adhere to the surface of the parts.

All tested samples saw an increase in the contact angle of water, indicating a reduction in the material’s surface energy. For example, the sample with 1% saw an increase of 13.5°, while the 2% and 7.5% samples saw an increase of 8°. The most significant improvement was at the 5% concentration with a contact angle of 69.5°. The comparison between the control and 5% ZnO sample is depicted in Figure 3.

3.3. SEM Imaging

SEM was conducted to identify the dispersion and agglomeration characteristics of the nanocomposites. This allowed for the inspection of particle size, agglomeration, dispersion, and EDS analysis. Along with this, it allowed for the documentation of voids and imperfections caused due to increase in ZnO concentration. To prepare the samples for high vacuum SEM, all samples were coated with iridium at 2–5 nanometers. Beyond this, the samples were imaged as printed.

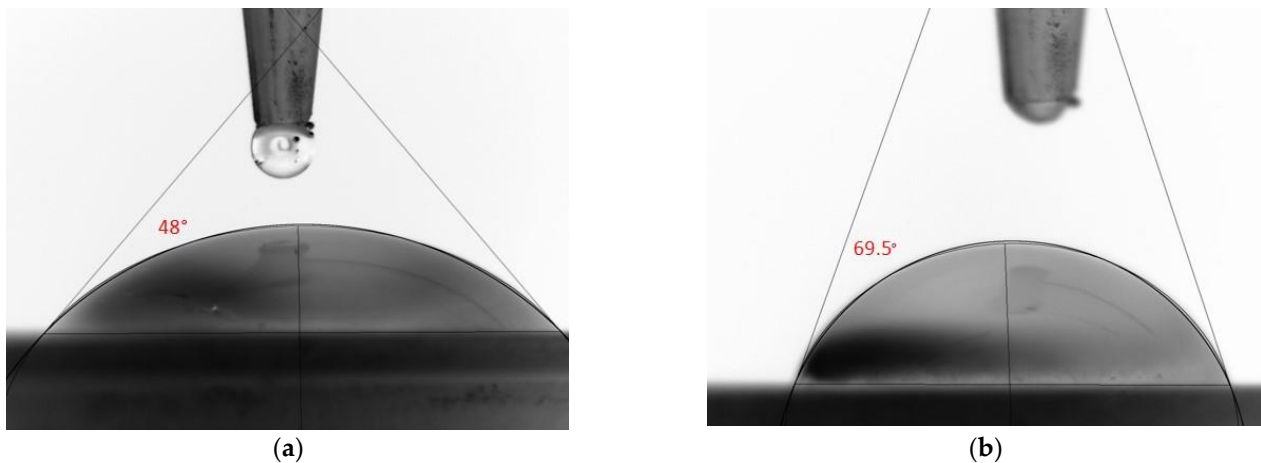


Figure 3. (a) Water contact angle of the control sample. (b) Water contact angle of the 5% ZnO sample.

To investigate agglomeration of the ZnO, EDS was performed on the specimens, and then particle analysis through ImageJ was performed. Figure 4 depicts this process with a backscatter image of a ZnO sample of 2.5% weight concentration with the white agglomerations representing the ZnO. All images processed provided a rough estimate of surface coverage, demonstrating an increase in coverage with ZnO concentration. Based on Figure 4b, it was also noted that large agglomerations were present but did not prevent an even coverage of the material's surface. As backscatter imagery was used at a 15 kV accelerating voltage, these images depict the layer up to several microns under the surface providing evidence for 3D dispersion of the ZnO.

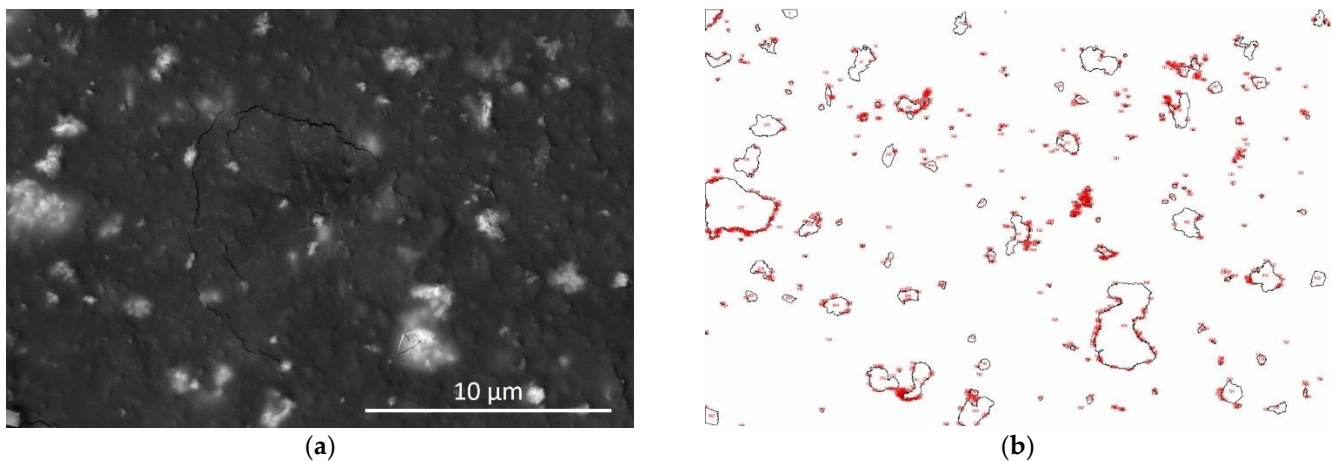


Figure 4. (a) SEM backscatter imagery of 2.5% ZnO sample. (b) Particle analysis using ImageJ demonstrating surface agglomerations.

Inspection of the samples at magnifications above $5000\times$ begins to show geometrical voids and issues with samples at and above 5% in multiple locations of the sample. To adequately identify the makeup of the sample, EDS was performed on the samples with 1% ZnO weight concentration (Figure 5a) and 5% ZnO weight concentration (Figure 5b). In Figure 5a, the number 1 inspection point provided a weight percentage of 57.4% for Zn while being completely absent at inspection point 2. Along with this, the sample's surface lacks voids and surface roughness. Comparatively, the 5% sample in Figure 5b, shows multiple voids and surface defects, although the concentration of zinc was much higher. The void was verified through EDS, with inspection point 5 returning a complete lack of Zn. Inspection points 1 through 4 returned varying weight percentages of Zn ranging from 25.9% to 58.6%. This meets theoretical expectations based on the interaction volume of

the electron beam picking up X-rays from below the ZnO agglomeration. Based on these results, the main concern is the voids' effect on the strength and the reduction in the ability to qualify the process over mass manufacturing.

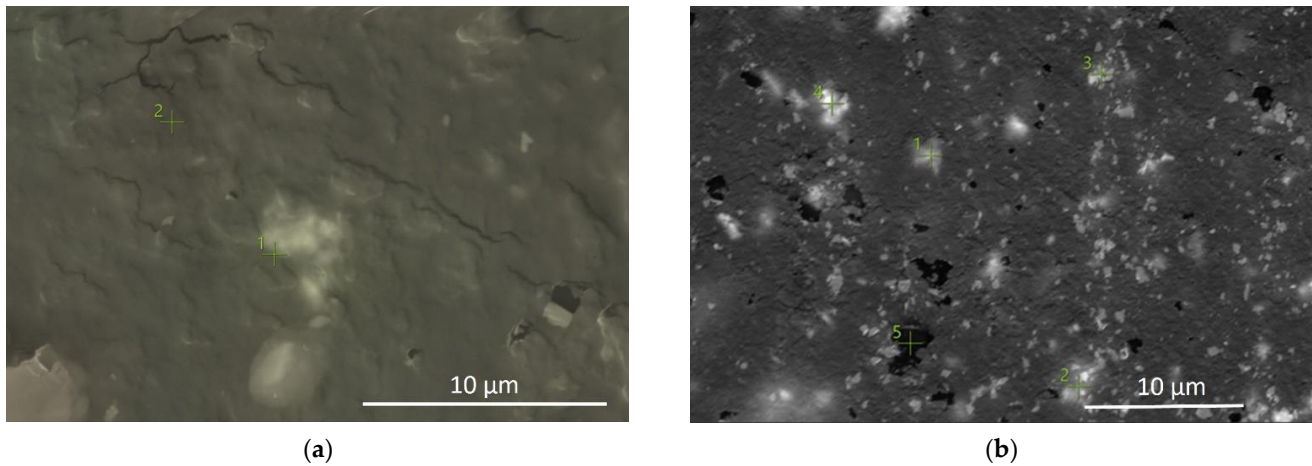


Figure 5. (a) SEM backscatter imagery of 1% ZnO sample with EDS inspection points at markers. (b) EDS analysis of 5% ZnO sample validating voids and ZnO agglomerations.

3.4. Sporocidal Effects

We summarized the sporocidal effects of nanocomposites in Table 3. Average colonies were 273.5 ± 47.4 , 260.5 ± 41.7 , and 178 ± 5.66 , respectively, which in turn, resulting 27,350, 26,050, and 17,800 spores per mL recovered. Compared to the control, ZnO nanocomposite reduced 31.5% of *C. difficile* spores. The samples are significantly different, with a p -value of 0.0031. Tukey multiple pairwise comparisons indicated that ZnO nanocomposite demonstrated reduction compared to baseline ($p = 0.123$) and control ($p = 0.18$). Although Levene's test outputs $p < 0.0001$, since ANOVA F-tests on an essentially perfect fit are unreliable, we can ignore this result and assume that we have homogeneity of variances in the different groups. The conclusion of the Q-Q plot is supported by the Shapiro–Wilk test on the ANOVA residuals ($W = 0.918$, $p = 0.4166$), which finds no violation of the normality assumption.

Table 3. *C. difficile* colony counting.

Baseline	Control (Polymer Only)	ZnO Nanocomposite
273.5 ± 47.4	260.5 ± 41.7	178 ± 5.66

4. Discussion

The main advantage of designing a nanocomposite utilizing ZnO is the presented antibacterial properties but increases in mechanical strength were also witnessed. A disadvantage addressed in this study was the effect of the UV absorbing nanoparticle when introduced into a thermoset cured at these wavelengths. ZnO nanoparticles from 15–40 nanometers have been documented to absorb UV wavelengths [22]. This absorption of UV light directly affected the required cure times and defects in the specimens. The tensile tests performed gave insight into the nanoparticle's effect on the material's strength and stiffness. Further investigation utilizing SEM provided insights into failure modes and dispersion characteristics.

Ideal applications for this material would be in heavily trafficked areas with a large volume of human contact. Specific applications include dental implants, prosthetic appendages, and high contact hardware such as doorknobs. Additionally, a reduction in strain is often required in items such as dental implants and prosthetics, as unwanted deflection can cause discomfort for the user. This technology is best suited for creating

one-off parts that cannot be traditionally manufactured and require complex geometry. Introducing the nanoparticle at a 1% concentration reduced ultimate tensile strength and stiffness compared to the control. This is likely due to the addition of the ZnO causing minor defects in the sample and, at such a low concentration, not being able to make up for those defects mechanically. This theory further presents itself when analyzing the 2.5% and 5% concentrations, as the strength and stiffness increase linearly.

The ZnO agglomerations can be measured in the SEM images in Figures 4 and 5. A void would be defined as a pocket of resin left uncured due to improper light exposure. The creation of voids increases with ZnO agglomeration size as the overall UV absorption per unit area increases. Utilizing SEM images, many agglomerations were documented to fall under 2 microns in diameter. When utilizing a layer height of 50 microns, a stack up of 2-micron agglomerations would gradually absorb the UV light as it travels vertically through the layer. This would lead to increased voids as nanoparticle concentration increases. This was demonstrated in Figure 5, with the 5% sample having significantly more voids than the lower 1% concentration samples. These voids would soon reach an equilibrium where the mechanical strength added due to the nanoparticle would be non-evident due to the void count. Additionally, the larger the voids present, the increased probability that the sample would fail prematurely, leading to a larger standard deviation concerning tensile stress. This problem appears to happen in the 7.5% ZnO concentrations, where the tensile strength is statistically similar to the 5% sample when considering standard deviation, but the modulus of the material is reduced. This increase in strain rate is a key indicator of larger defects within the sample that also increase the large strength variability, as seen by the error bars in Figure 2. Optical microscope images were taken of the fracture point of several samples to provide more insight into the failure mechanism, as seen in Figure 6.

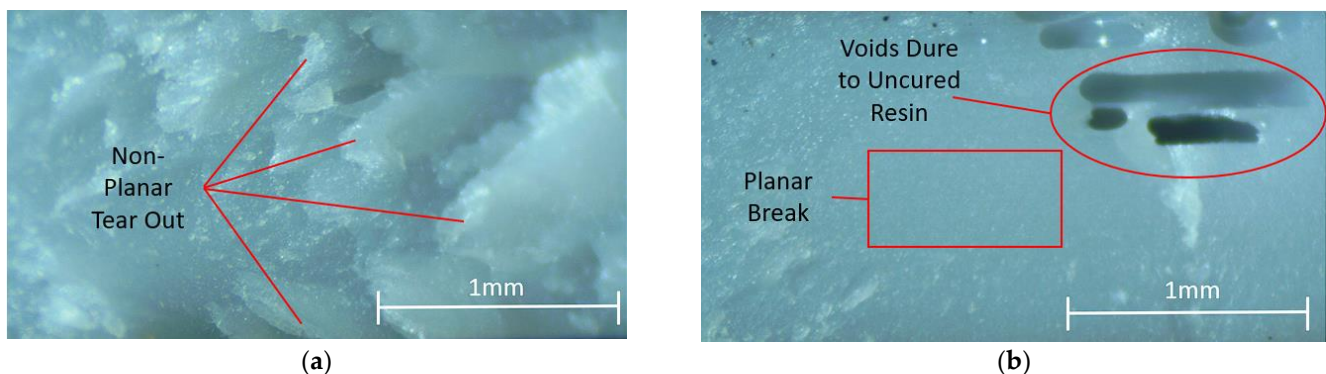


Figure 6. (a) Optical microscope image of fracture point of 7.5% sample (b) Optical microscope image of fracture due to voids on 7.5% sample.

The image in Figure 6a was taken of a sample that fell within the range of expected tensile values as provided by the data. Obvious tear-out can be observed with a nearly crystalline structure being left behind. The image in Figure 6b was taken of a sample that failed prematurely with large voids. The images are presented with the z-axis traveling vertically through the images. No layer lines are visible, but the voids appear to have formed within several consecutive layers leading to a weakened sample. An important note is that the fracture point on the defective sample shows no tear out and resembles a smooth surface indicating that the point at which the ZnO became the functional mechanical structure was never reached.

The presented data lead to the theory that ZnO addition to a UV curable resin matrix increases the part's mechanical properties up to 25%. This considers the failure in achieving a defect-free sample and therefore allows for future research in processes to reduce the void count. SEM images for samples up to 2.5% demonstrated no concerning void creation near or around the ZnO. At and above 5%, these voids became very apparent and were

often located near a large agglomeration of ZnO. As ZnO absorbs the UV, it is suspected that the imaged voids are uncured resin surrounding larger ZnO groups. Possible solutions to this issue would be to reduce layer height and increase energy density per unit volume of the nanocomposite. Increasing the dispersion of the ZnO specifically through methods such as tip sonication to help overcome the surface energy of the particles should also be further investigated. Lastly, performing thermal studies on the temperature and viscosity of the nanocomposite during the printing process would likely lead to improved part performance.

In addition, this study is the first of evaluating the sporicidal effects of ZnO nanocomposite on *C. difficile*. The present work provides experimental evidence that the nanocomposites reduce *C. difficile* counts within contact in 24 h. *C. difficile* is a major health threat that can easily spread and contaminate environmental surfaces. Even if Paired Comparison did not show a statistical indication due to the small sample size, continued experiments in the future would most likely demonstrate a significant difference by increasing the sample size. Given the significant reduction in spores caused by nanocomposites, promoting the evaluations of other nanocomposites and their further basic and applied research are needed.

5. Conclusions

Additive manufacturing allows for implementing unique design ideas and products not possible with traditional manufacturing. Creating a novel nanocomposite that integrates into market available printing systems with improved mechanical and chemical characteristics offers great promise for helping alleviate these issues. Nanocomposites open an important sector in additive manufacturing as once the material is created; it can be utilized in nearly any system. By adding zinc oxide into a photocurable resin utilized in SLA-based printing systems, a novel nanocomposite could be created that offers antibacterial properties while significantly increasing the part's strength and stiffness. Up to nearly a 25% increase in ultimate tensile strength and 35% increase in modulus was achieved through just a 5% weight concentration of this nanoparticle. This low concentration allowed for minimal printing parameter adjustments and reduced part failure compared to larger reinforcement to matrix ratios. This material's applications include custom prosthetics, dental implants, and hospital tools and fixtures. Due to the antimicrobial features offered, complex geometries can be produced that often lead to bacterial growth issues in other parts. In addition, the added stiffness to the parts will allow for an increased tensile load as the elastic region extends compared to control groups. While additive manufacturing is still struggling to reach widespread adoption, the research into composite-based materials will allow for novel use cases that require implementing these technologies. The future of additive manufacturing will be in material science and composite research to create parts that offer secondary functions without secondary processing requirements. The antibacterial function offered by these parts will not wear off compared to many coatings and surface applications as the ZnO will continue to be exposed to the surface regardless of part wear over time. The future steps for this research would include qualification processes and further adjustments to printing environments to maximize part quality and strength.

Author Contributions: Conceptualization, Y.L., C.C. and J.D.B.; methodology, C.B., T.S. and P.K.; writing—original draft preparation, C.B.; writing—review and editing, Y.L., C.C. and J.D.B. All authors have read and agreed to the published version of the manuscript.

Funding: This research was funded by the Presbyterian Health Foundation (PHF), grant number 20002136. The authors also appreciate the financial support provided by the Vice President for Research and Partnerships office at the University of Oklahoma.

Data Availability Statement: Data available on request.

Conflicts of Interest: The authors declare no conflict of interest. The funders had no role in the design of the study; in the collection, analyses, or interpretation of data; in the writing of the manuscript, or in the decision to publish the results.

References

1. Blanco, I. The use of composite materials in 3D printing. *J. Compos. Sci.* **2020**, *4*, 42. [[CrossRef](#)]
2. Quan, H.; Zhang, T.; Xu, H.; Luo, S.; Nie, J.; Zhu, X. Photo-curing 3D printing technique and its challenges. *Bioact. Mater.* **2020**, *5*, 110–115. [[CrossRef](#)] [[PubMed](#)]
3. Mendes-Felipe, C.; Oliveira, J.; Etxebarria, I.; Vilas-Vilela, J.L.; Lanceros-Mendez, S. State-of-the-art and future challenges of UV curable polymer-based smart materials for printing technologies. *Adv. Mater. Technol.* **2019**, *4*, 1800618. [[CrossRef](#)]
4. Parandoush, P.; Lin, D. A review on additive manufacturing of polymer-fiber composites. *Compos. Struct.* **2017**, *182*, 36–53. [[CrossRef](#)]
5. Herren, B.; Saha, M.C.; Altan, M.C.; Liu, Y. Development of ultrastretchable and skin attachable nanocomposites for human motion monitoring via embedded 3D printing. *Compos. Part B Eng.* **2020**, *200*, 108224. [[CrossRef](#)]
6. Abshirini, M.; Charara, M.; Liu, Y.; Saha, M.; Altan, M.C. 3D printing of highly stretchable strain sensors based on carbon nanotube nanocomposites. *Adv. Eng. Mater.* **2018**, *20*, 1800425. [[CrossRef](#)]
7. Singh, S.; Ramakrishna, S.; Berto, F. 3D Printing of polymer composites: A short review. *Mater. Des. Process. Commun.* **2020**, *2*, e97. [[CrossRef](#)]
8. Ding, Y.; Yang, I.S.; Li, Z.; Xia, X.; Lee, W.I.; Dai, S.; Bahnmann, D.W.; Pan, J.H. Nanoporous TiO₂ spheres with tailored textural properties: Controllable synthesis, formation mechanism, and photochemical applications. *Prog. Mater. Sci.* **2020**, *109*, 100620. [[CrossRef](#)]
9. Shekofteh-Gohari, M.; Habibi-Yangjeh, A.; Abitorabi, M.; Rouhi, A. Magnetically separable nanocomposites based on ZnO and their applications in photocatalytic processes: A review. *Crit. Rev. Environ. Sci. Technol.* **2018**, *48*, 806–857. [[CrossRef](#)]
10. Abebe, B.; Zereffa, E.A.; Tadesse, A.; Murthy, H. A review on enhancing the antibacterial activity of ZnO: Mechanisms and microscopic investigation. *Nanoscale Res. Lett.* **2020**, *15*, 190. [[CrossRef](#)]
11. Marashizadeh, P.; Abshirini, M.; Saha, M.; Huang, L.; Liu, Y. Functionalization Enhancement on Interfacial Properties between Graphene and ZnO NW/Epoxy: A Molecular Dynamics Simulation Study. *Adv. Theory Simul.* **2022**, *5*, 2200010. [[CrossRef](#)]
12. Lin, Y.; Ehlert, G.; Sodano, H.A. Increased interface strength in carbon fiber composites through a ZnO nanowire interphase. *Adv. Funct. Mater.* **2009**, *19*, 2654–2660. [[CrossRef](#)]
13. Marashizadeh, P.; Abshirini, M.; Saha, M.; Huang, L.; Liu, Y. Interfacial Properties of ZnO Nanowire-Enhanced Carbon Fiber Composites: A Molecular Dynamics Simulation Study. *Langmuir* **2021**, *37*, 7138–7146. [[CrossRef](#)] [[PubMed](#)]
14. Wang, J.; Marashizadeh, P.; Weng, B.; Larson, P.; Altan, M.C.; Liu, Y. Synthesis, Characterization, and Modeling of Aligned ZnO Nanowire-Enhanced Carbon-Fiber-Reinforced Composites. *Materials* **2022**, *15*, 2618. [[CrossRef](#)]
15. Shi, L.-E.; Li, Z.-H.; Zheng, W.; Zhao, Y.-F.; Jin, Y.-F.; Tang, Z.-X. Synthesis, antibacterial activity, antibacterial mechanism and food applications of ZnO nanoparticles: A review. *Food Addit. Contam. Part A* **2014**, *31*, 173–186. [[CrossRef](#)]
16. Da Silva, B.L.; Caetano, B.L.; Chiari-Andréo, B.G.; Pietro, R.C.L.R.; Chiavacci, L.A. Increased antibacterial activity of ZnO nanoparticles: Influence of size and surface modification. *Colloids Surf. B Biointerfaces* **2019**, *177*, 440–447. [[CrossRef](#)]
17. Yamamoto, O. Influence of particle size on the antibacterial activity of zinc oxide. *Int. J. Inorg. Mater.* **2001**, *3*, 643–646. [[CrossRef](#)]
18. Raghupathi, K.R.; Koodali, R.T.; Manna, A.C. Size-dependent bacterial growth inhibition and mechanism of antibacterial activity of zinc oxide nanoparticles. *Langmuir* **2011**, *27*, 4020–4028. [[CrossRef](#)]
19. Qi, K.; Cheng, B.; Yu, J.; Ho, W. Review on the improvement of the photocatalytic and antibacterial activities of ZnO. *J. Alloys Compd.* **2017**, *727*, 792–820. [[CrossRef](#)]
20. El-Megharbel, S.M.; Alsawat, M.; Al-Salmi, F.A.; Hamza, R.Z. Utilizing of (zinc oxide nano-spray) for disinfection against “SARS-CoV-2” and testing its biological effectiveness on some biochemical parameters during (COVID-19 pandemic)—“ZnO nanoparticles have antiviral activity against (SARS-CoV-2)”. *Coatings* **2021**, *11*, 388. [[CrossRef](#)]
21. Sirelkhatim, A.; Mahmud, S.; Seeni, A.; Kaus, N.H.M.; Ann, L.C.; Bakhori, S.K.M.; Hasan, H.; Mohamad, D. Review on zinc oxide nanoparticles: Antibacterial activity and toxicity mechanism. *Nano Micro Lett.* **2015**, *7*, 219–242. [[CrossRef](#)] [[PubMed](#)]
22. Peery, A.F.; Dellon, E.S.; Lund, J.; Crockett, S.D.; McGowan, C.E.; Bulsiewicz, W.J.; Gangarosa, L.M.; Thiny, M.T.; Stitzenberg, K.; Morgan, D.R. Burden of gastrointestinal disease in the United States: 2012 update. *Gastroenterology* **2012**, *143*, 1179–1187.e1173. [[CrossRef](#)] [[PubMed](#)]
23. Saito, M. Antibacterial, deodorizing, and UV absorbing materials obtained with zinc oxide (ZnO) coated fabrics. *J. Coat. Fabr.* **1993**, *23*, 150–164. [[CrossRef](#)]
24. Goh, E.; Xu, X.; McCormick, P. Effect of particle size on the UV absorbance of zinc oxide nanoparticles. *Scr. Mater.* **2014**, *78*, 49–52. [[CrossRef](#)]
25. Ramezanzadeh, B.; Attar, M.; Farzam, M. Effect of ZnO nanoparticles on the thermal and mechanical properties of epoxy-based nanocomposite. *J. Therm. Anal. Calorim.* **2011**, *103*, 731–739. [[CrossRef](#)]
26. Nowacki, B.; Kowol, P.; Koziol, M.; Olesik, P.; Wiczorek, J.; Waclawiak, K. Effect of Post-Process Curing and Washing Time on Mechanical Properties of mSLA Printouts. *Materials* **2021**, *14*, 4856. [[CrossRef](#)]
27. Lee, M.; Kwak, G.; Yong, K. Wettability control of ZnO nanoparticles for universal applications. *ACS Appl. Mater. Interfaces* **2011**, *3*, 3350–3356. [[CrossRef](#)]
28. Ren-De Sun, A.N.; Akira, F.; Toshiya, W.; Kazuhito, H. Photoinduced surface wettability conversion of ZnO and TiO₂ thin films. *J. Phys. Chem. B* **2001**, *105*, 1984–1990.

29. Park, J.-M.; Ahn, J.-S.; Cha, H.-S.; Lee, J.-H. Wear resistance of 3D printing resin material opposing zirconia and metal antagonists. *Materials* **2018**, *11*, 1043. [[CrossRef](#)]
30. Billings, C.; Cai, C.; Liu, Y. Utilization of antibacterial nanoparticles in photocurable additive manufacturing of advanced composites for improved public health. *Polymers* **2021**, *13*, 2616. [[CrossRef](#)]
31. Herren, B.; Saha, M.C.; Altan, M.C.; Liu, Y. Funnel-Shaped Floating Vessel Oil Skimmer with Joule Heating Sorption Functionality. *Polymers* **2022**, *14*, 2269. [[CrossRef](#)] [[PubMed](#)]
32. Wang, J.; Weng, B.; Larson, P.; Liu, Y. Synthesis and characterization of self-assembled ZnO nanoarrays on hybrid structural fibers. *Surf. Interfaces* **2019**, *16*, 188–193. [[CrossRef](#)]
33. Martín-Montal, J.; Pernas-Sánchez, J.; Varas, D. Experimental characterization framework for SLA additive manufacturing materials. *Polymers* **2021**, *13*, 1147. [[CrossRef](#)] [[PubMed](#)]